J. Fluid Mech. (1965), *vol.* 23, *part* 4, *pp.* 689–713
Printed in Great Britain

On some aspects of fully-developed turbulent flow in rectangular channels

By F. B. GESSNER† AND J. B. JONES†
School of Mechanical Engineering, Purdue University

(Received 4 March 1965)

For fully-developed turbulent flow in straight channels of non-circular cross-section, there exists a transverse mean flow superimposed upon the axial mean flow. This transverse flow, commonly known as secondary flow, interacts with the axial mean flow and turbulence structure in a complex manner. In this paper several heretofore unexplored aspects of this type of secondary flow are discussed on the basis of results of an extensive experimental programme which was conducted for steady, incompressible, fully-developed turbulent air flow in both square and rectangular channels. Specifically, the following aspects are examined: (*a*) the Reynolds-number effect on secondary flow, (*b*) the directional characteristics of local wall shear stress, (*c*) the orientation of Reynolds-stress principal planes in a plane normal to the axial flow direction, and (*d*) the Reynolds equation along a secondary-flow streamline.

Within the Reynolds-number range of the investigation, the results indicate that secondary-flow velocities, when non-dimensionalized with either the bulk velocity or the axial mean-flow velocity at the channel centreline, decrease for an increase in Reynolds number. Also, the greatest skewness of local wall shear-stress vectors is shown to occur in the near vicinity of corners where secondary flow is maximum. In addition, it is shown that in planes normal to the axial flow direction, traces of Reynolds stress principal planes are not tangent and normal to lines of constant axial mean-flow velocity. This behaviour is in contrast to that for less complicated turbulent flows, for example, two-dimensional channel flow or circular-pipe flow where such traces are always tangent and normal to lines of constant axial mean-flow velocity in accordance with symmetry considerations. Finally, through experimental evaluation of terms in a momentum balance along a typical secondary-flow streamline, it is shown that secondary flow is the result of small differences in magnitude of opposing forces exerted by the Reynolds stresses and static pressure gradients in planes normal to the axial flow direction.

1. Introduction

Fully-developed turbulent flow in straight channels of non-circular cross-section is three-dimensional in both mean-flow and turbulence structure. The mean-flow velocity vector at each point in the flow field is generally composed of a component in the axial flow direction and transverse components in a plane

† Now at Virginia Polytechnic Institute, Blacksburg, Virginia.

normal to this direction. The transverse components at all points form a flow pattern known as secondary flow which can be regarded as superimposed upon the axial mean flow.

For fully-developed laminar flow in straight non-circular channels secondary flow is non-existent. This can be shown analytically (Moissis 1957; Maslen 1958) and has been verified experimentally by Oman (1959) for the particular case of laminar flow in a square channel.

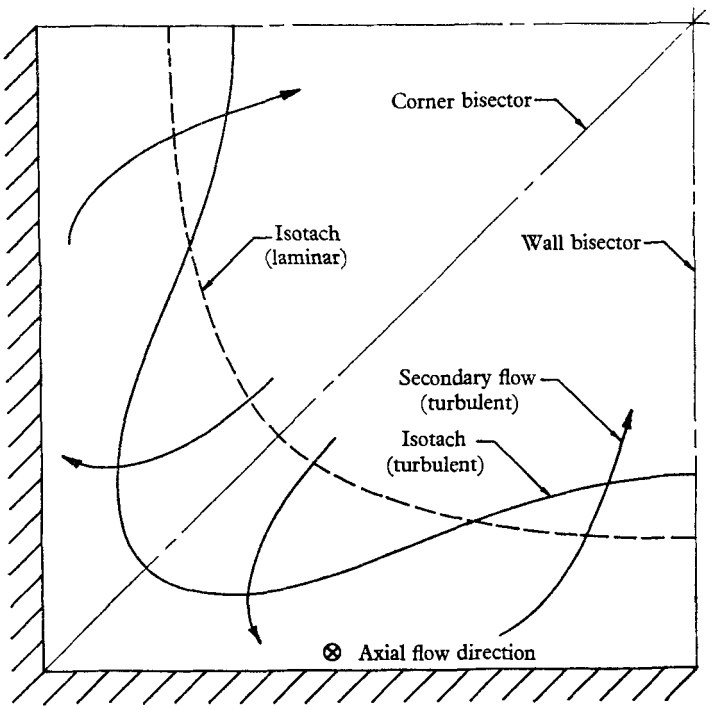

FIGURE 1. Typical isotach patterns in a square channel.

For discussion purposes let us consider fully-developed turbulent flow in a square channel. From experimental measurements it is known that secondary flow in this type of channel distorts isotachs as shown in figure 1, where an isotach is defined to be a line of constant axial mean-flow velocity in a plane normal to the axial flow direction. For comparison purposes a typical isotach for fully-developed laminar flow is also shown in figure 1. If quantitative measurements of secondary flow are made, it is possible to construct so-called secondary-flow streamlines. Typical secondary-flow streamline patterns are shown in figure 2 where Ψ is a stream function to be defined later and $C_1, C_2, \ldots$ are constant values.

Secondary flow in straight channels of non-circular cross-section was first observed by Nikuradse (1926) who made careful measurements of isotach distributions in several channel geometries and found isotachs to be distorted in a manner indicative of secondary flow. More recently, Hoagland (1960) measured complete mean-flow velocity distributions for fully-developed turbulent flow in a square channel. Similar measurements were made by Gilbert (1960) in a

rectangular channel. The results of both investigators indicate typical secondary-flow velocities on the order of 1% of the maximum axial mean-flow velocity, and furthermore show that secondary flow, although a small fraction of the total mean flow, has a pronounced effect on isotach distributions. Hoagland also

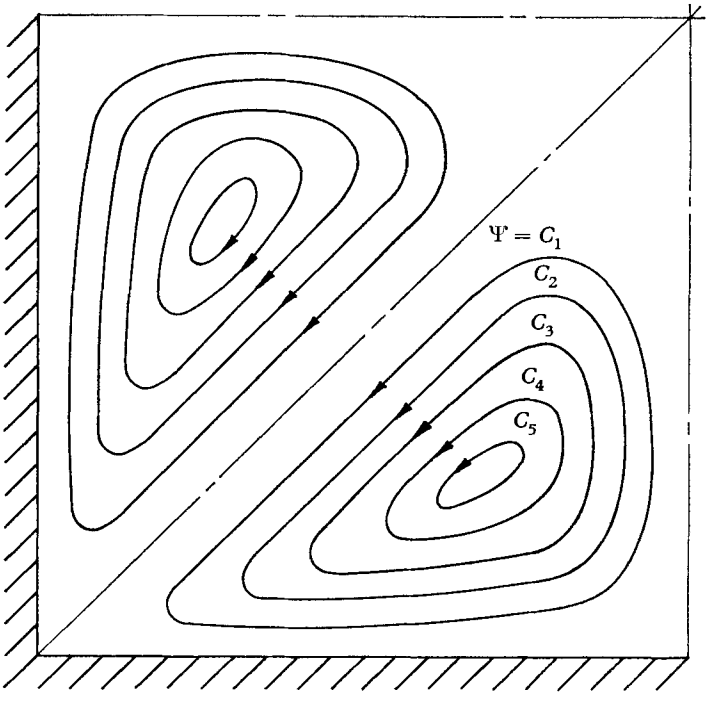

FIGURE 2. Typical secondary-flow streamline patterns in a square channel.

determined the local wall shear-stress distribution in a square channel by direct measurements with a Preston tube. Subsequently, Leutheusser (1963) presented local wall shear-stress distributions in a rectangular channel. Both Hoagland and Leutheusser, however, measured only magnitudes of local wall shear-stress and not directional characteristics. The latter aspect should be included in any measurements of local wall shear-stress in non-circular channels because the wall shear-stress vectors are skewed as a consequence of secondary flow. Brundrett (1964) examined secondary flow in square and rectangular channels from a vorticity standpoint. His experimental work included measurement of all six components of the Reynolds-stress tensor as well as mean-flow velocity distributions. Through experimental evaluation of terms in the axial vorticity equation, Brundrett showed that convection and diffusion of secondary-flow vorticity are balanced approximately by the production of vorticity from the Reynolds stresses.

Even though recent work has shed considerable light on the phenomenon of secondary flow, there are still several unexplored aspects that merit consideration. For example, the Reynolds-number effect on secondary flow and the directional characteristics of local wall shear stress have not been measured. In addition, certain properties of the Reynolds-stress tensor have not been

examined, namely the orientation of traces of Reynolds-stress principal planes in planes normal to the axial-flow direction. In two-dimensional channel flow and circular-pipe flow, for example, such traces are always tangent and normal to isotachs in accordance with symmetry considerations; but when isotachs are distorted by secondary flow, no such direct conclusion is possible. It is of interest, therefore, to examine this characteristic of the turbulence structure for comparison with the structure associated with less complicated flows. Another unexplored aspect is a determination of the forces causing secondary flow from a momentum standpoint. This aspect can be analysed by writing the Reynolds equation along a secondary-flow streamline in streamline co-ordinates, and then experimentally evaluating each term in the equation along selected secondary-flow streamlines. This procedure enables one to determine the predominant forces causing fluid motion along secondary-flow streamlines, i.e. the actual driving mechanism of secondary flow. Of course, the last two aspects can be analysed in some detail by applying a co-ordinate-axes transformation to Brundrett's data. However, such a technique is not practical, and hence direct measurements with respect to isotachs and secondary-flow streamlines must be made.

The intent of this paper is to help complete the state of knowledge about secondary flow through presentation of experimental results relating to the above-mentioned aspects. The original intent was also to include results in the form of measured Reynolds-stress distributions in both square and rectangular channels. The recent work of Brundrett, however, presents such results and for this reason the present authors' results are omitted, although it should be noted that the two works complement each other since different Reynolds numbers are considered. That work which does not overlap is presented herein and is based on the doctoral thesis of the senior author (Gessner 1964*a*). For steady, incompressible, fully-developed turbulent air-flow in both square and rectangular channels the following aspects are examined: (i) the Reynolds-number effect on secondary flow; (ii) the directional characteristics of local wall shear stress; (iii) the orientation of traces of Reynolds-stress principal planes in a plane normal to the axial flow direction; (iv) the Reynolds equation along a secondary-flow streamline.

2. Flow system

A schematic diagram of the flow system is shown in figure 3. Room air was drawn into the channel through circular tubes at the inlet to minimize swirl. The inlet was followed by a contraction and then by a honeycomb to help stabilize the flow. Turning vanes were placed in sections where the main flow was turned to ensure further a stable flow. The flow rate was adjusted either by inducting room air into the system downstream of the measuring station or by adjusting a sliding by-pass valve on the discharge side of the centrifugal fan. The layout of the overall configuration as shown in the figure was necessary because the fan position was fixed and maximum channel length was desired.

The channel was constructed with one adjustable wall which was moved to change the aspect ratio of the channel cross-section. All four walls of the channel were made of Formica bonded to $\frac{5}{8}$ in. flakeboard. Turnbuckles were located at 2 tf. intervals along the channel to tighten the adjustable wall in place. Epoxy

resin was used on all permanent seams, and electrical tape on the seams between the adjustable and fixed walls to ensure a leakage-free system.

Initially, the adjustable wall was positioned so that the channel cross-section was 8 in. square. The corresponding L/D_h ratio was 40, where L denotes the channel length between the inlet and the measuring station, and D_h, the hydraulic diameter of the channel. In order to promote rapid boundary-layer development, the boundary layer was tripped by $\frac{1}{8}$ in. diameter wires at the inlet and artificially thickened by screens immediately behind the trip wires. The screen configuration consisted of three different mesh screens, and the solidity ratio of the configura-

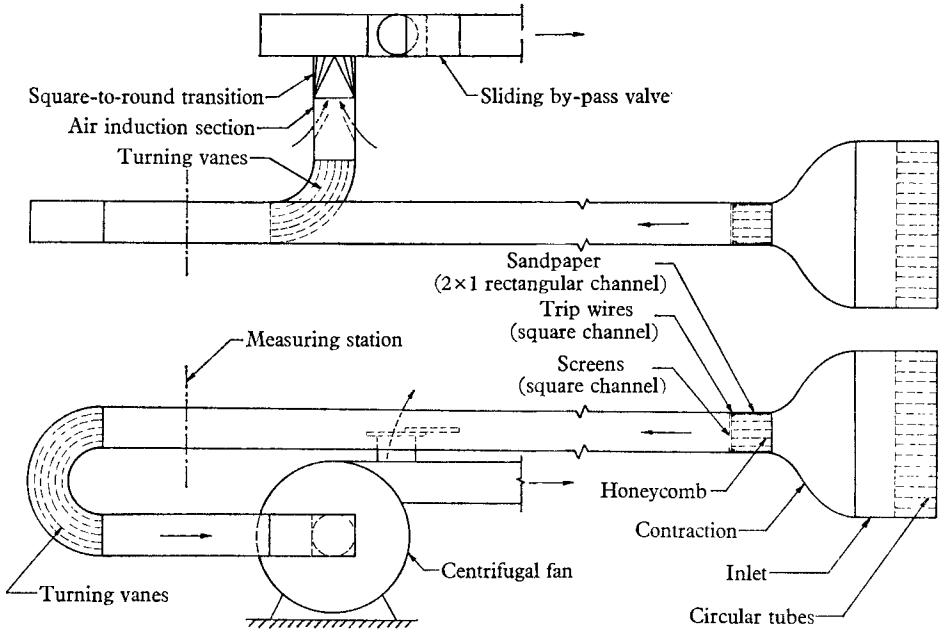

FIGURE 3. Schematic diagram of flow system.

tion increased toward the wall. This configuration severely restricted the flow and consequently limited measurements to a narrow Reynolds-number range; however, it was necessary to ensure fully-developed flow at the measuring station. In fact, without the screens of varying solidity near the inlet, a much higher value of L/D_h would have been needed for the attainment of fully-developed flow.

After experimental measurements in the square channel had been completed, the adjustable wall was moved toward the opposite wall until the cross-section was 8 in. × 4 in., giving an aspect ratio of 2 and an L/D_h ratio of 60. For the 2 × 1 rectangular channel the trip wires and screens at the inlet were removed and replaced by a 6 in. wide strip of no. 3 grit sandpaper around the channel periphery. The sandpaper was effective in tripping the boundary layer and in promoting boundary-layer growth to ensure fully-developed flow at the measuring station. The primary reason for replacing the trip wires and screens with sandpaper was to reduce the flow losses associated with the screen configuration and, in turn, to permit measurements to be taken over a wider Reynolds-number range.

3. Instrumentation

Static pressure taps and access holes for a total head tube and single-wire and X-array hot-wire anemometer probes were located immediately upstream of the honeycomb at the inlet and at 1 ft. intervals upstream of the measuring station for a distance of 3 ft. At the measuring station a traversing mechanism was used to position the total head tube and hot-wire probes. A rack and pinion arrangement and a screw mechanism provided translation normal to the axial flow direction (x-direction) in two mutually perpendicular directions aligned with the channel walls (y- and z-directions).

Axial mean-flow velocity measurements were made with the total head tube in conjunction with a wall static-pressure tap in the same transverse plane on the opposite wall. A probing of the flow field with a Pitot static tube indicated that the error involved in the use of a wall tap for these measurements was negligible over the Reynolds-number range of the investigation. In order to measure secondary-flow velocity components quantitatively, the single-wire rotation method described by Hoagland (1960) was used. A modified form of Hoagland's bridge circuit was employed to make possible accurate measurements in the region of high turbulence intensity near a wall. Directional characteristics of local wall shear stress were determined with a specially designed hot-wire instrument. Details of the instrumentation and techniques used are given by Gessner (1964*a*).

Turbulence measurements were made with a single-wire probe and with an X-wire probe. The wires of both probes were made of tungsten, 0·00015 in. in diameter, and 0·04 in. in length. The wires of the X-array were approximately 0·02 in. apart, and the included angle between the wires was 90°. At the measuring station both types of probes were mounted parallel to the x-direction to minimize probe stem interference. Since the plane of the X-array was also parallel to the x-direction, a rotation of the X-wire probe permitted the X-array to be oriented in an xy- or xz-plane, or in any intermediate plane. The single-wire probe was used to measure normal stress in the x-direction. The other Reynolds stresses were measured consecutively at any one point with the X-wire probe in accordance with a method discussed by Gessner (1964*b*). A Flow Corporation constant-current hot-wire anemometer was used for all turbulence measurements.

4. Measurements

Mean-flow velocity and turbulence measurements were made in the square channel at Reynolds numbers of 75,000, 150,000 and 300,000, and in the 2×1 rectangular channel at Reynolds numbers of 50,000, 150,000 and 300,000. The Reynolds number is defined as $Re = D_h U_b/\nu$, where U_b is the bulk fluid velocity, ν the kinematic viscosity, and D_h is as previously defined.

Axial mean-flow velocity measurements were made just upstream of the honeycomb at the inlet to determine bulk velocities at various Reynolds numbers. Reynolds stress and axial mean-flow velocity measurements were also taken at 1 ft. intervals upstream of the measuring station to check for the existence of fully-developed flow at the station. In order to determine whether the flow was

symmetric in the cross-section at the measuring station, isotach distributions were determined, and secondary-flow components and the Reynolds stresses were measured at symmetrically located points in the entire cross-section. After symmetry of flow had been verified, detailed measurements of the flow structure were made.

5. Results and discussion

5.1. *Secondary-flow profiles*

Secondary-flow profiles measured in an octant of the square channel are shown in figures 4 and 5; those measured in a quadrant of the 2×1 rectangular channel are shown in figure 6. The results are presented in dimensionless form with

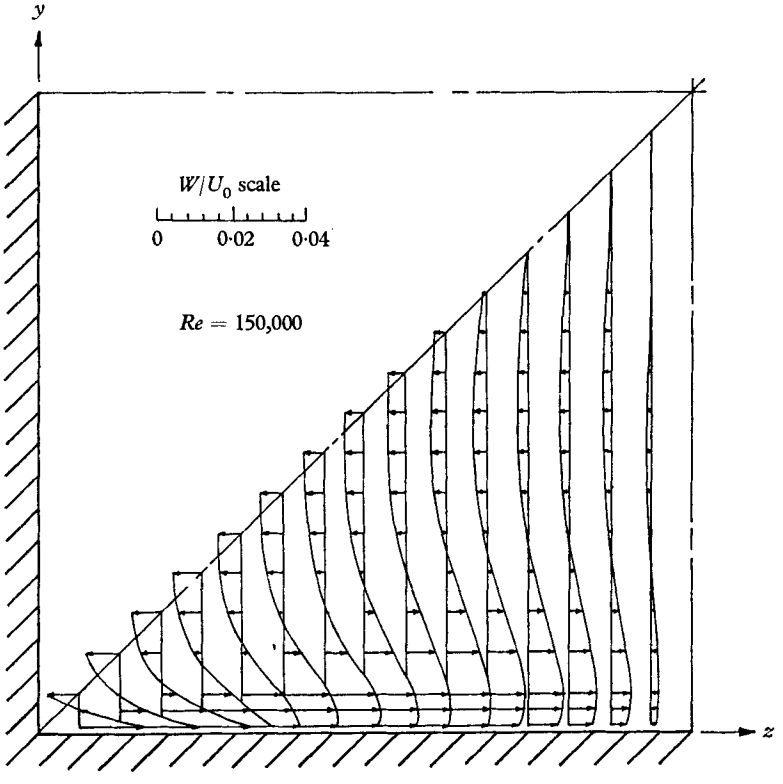

FIGURE 4. Secondary-flow profiles in a square channel.

W defined as the secondary-flow component in the z-direction and U_0 as the axial mean-flow velocity at the channel centreline. The magnitude and direction of each measured value of W/U_0 are indicated by the vectors shown in the figures and are based on an assumed zero value of W/U_0 along the wall bisector parallel to the y-direction, in accordance with symmetry considerations. It should be noted that only secondary-flow components in the z-direction were measured; for the purposes of this investigation it was not necessary to measure the y-direction component of secondary flow.

As indicated by figure 4, detailed measurements of W/U_0 profiles were made in

the square channel at $Re = 150{,}000$. This was done because the profiles shown in the figure were integrated in order to evaluate secondary-flow streamlines. A discussion follows later regarding the technique of determining secondary-flow streamlines from these profiles. In order to satisfy continuity, the difference

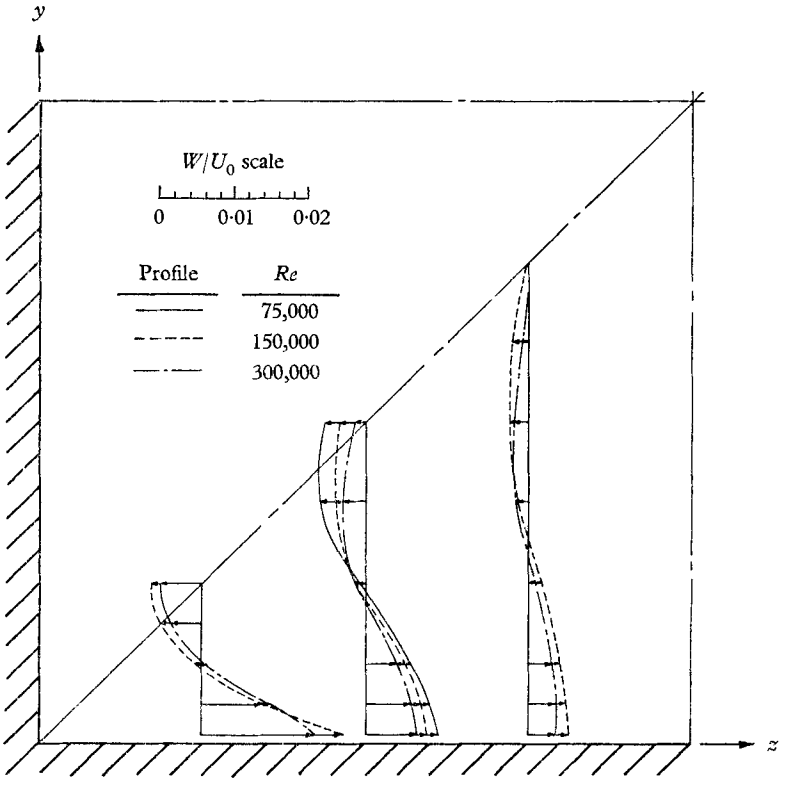

FIGURE 5. Secondary-flow profiles in a square channel over a range of Reynolds numbers.

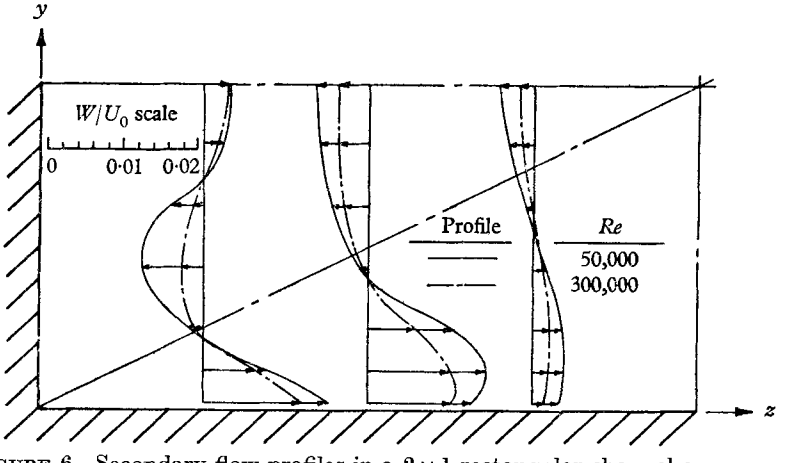

FIGURE 6. Secondary-flow profiles in a 2×1 rectangular channel over a range of Reynolds numbers.

between the average secondary-flow rate toward the wall $z = 0$ and that away from the wall should be zero for each profile. Careful examination of each profile indicates, however, an average flow rate away from the wall $z = 0$ which is approximately 20 % higher than that towards the wall. In order to determine the cause of this discrepancy, several possibilities were investigated. The possibility that room air was leaking into the channel at the corner joint was discounted because precautions had been taken to ensure a sealed system upstream of the measuring station. Another possibility involved the measurement of U, the local axial mean-flow velocity. Since the single-wire rotation method measures W/U, it was necessary to measure U at every secondary-flow measuring point in order to non-dimensionalize W in terms of the centreline velocity, U_0. It was therefore considered possible that measured values of U near the wall $y = 0$ were too high, resulting from displacement effects of the total-head tube on the flow. Displacement-effect corrections, however, did not explain the discrepancy. The procedure given by Rose (1962) for correcting mean-flow measurements in turbulent shear flow was also applied to measured values of W/U. The corrections had essentially no effect on the measured values. A final possibility considered was that values of W/U_0 on the wall bisector parallel to the y-axis were not actually zero. To investigate this possibility W/U_0 measurements were taken at symmetrically located points on either side of the wall bisector. The results indicated symmetric profiles within experimental accuracy and, consequently, that the zeroing procedure used in the measurements was correct. On the basis of the above considerations, the discrepancy could not be explained, and therefore no corrections were applied to the profiles shown in figure 4, nor to the profiles shown in figures 5 and 6, where the same type of discrepancy can be observed.

The Reynolds-number effect on secondary flow in the square channel and in the 2×1 rectangular channel can be seen in figures 5 and 6, respectively. Both figures indicate a decrease in secondary flow when non-dimensionalized with the centreline velocity for an increase in Reynolds number. Since the ratio of bulk velocity to centreline velocity was essentially constant ($U_b/U_0 \approx 0{\cdot}83$) over the Reynolds-number range considered for each channel, it also follows that secondary flow, when non-dimensionalized with the bulk velocity, decreases for an increase in Reynolds number. Measurements taken in the square channel at $Re = 150{,}000$ and 300,000 first indicated a decrease in secondary flow with increasing Reynolds number. Further measurements taken in the square channel at $Re = 75{,}000$ and in the 2×1 rectangular channel at $Re = 50{,}000$, 150,000 and 300,000 confirmed this trend. The effect is perhaps explained by increased turbulent mixing at high Reynolds numbers which tends to reduce gradients in the flow.

5.2. *Local wall shear-stress directional characteristics*

Directional characteristics of local wall shear stress measured in the square channel and in the 2×1 rectangular channel are shown in figures 7 and 8, respectively. Directional measurements were taken only at $Re = 300{,}000$ in both geometries because the hot-wire wall shear-stress instrument was not

sufficiently sensitive at lower Reynolds numbers for accurate measurements. Both figures 7 and 8 indicate that the skewness of wall shear-stress vectors τ_w increases as the corner is approached. In accordance with symmetry considerations the skewness of the wall stress vector at the corner should be zero. The

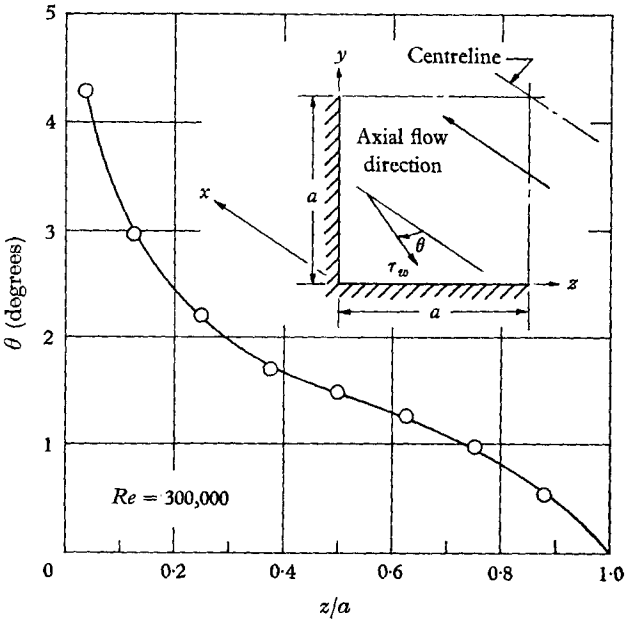

FIGURE 7. Directional characteristics of local wall shear-stress in a square channel.

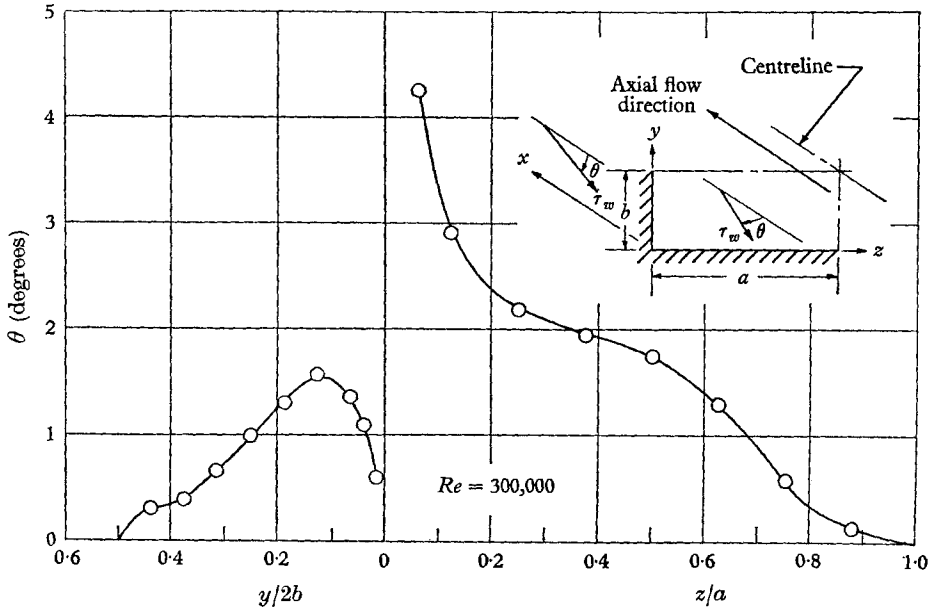

FIGURE 8. Directional characteristics of local wall shear-stress in a 2×1 rectangular channel.

tendency toward a zero value at the corner was observed along the shorter wall of the 2×1 rectangular channel, as is evident in figure 8. This tendency, however, was not detected along the longer wall nor in the square channel, because the instrument could not be positioned sufficiently close to the corner without damage to the sensing element. Figure 8 also shows that the skewness of wall stress vectors is greater along the longer wall than along the shorter wall of the 2×1 rectangular channel at points equidistant from the corner. This is in accordance with predictable behaviour based on the secondary-flow profiles shown in figure 6, from which it can be inferred that most of the flow away from the corner is directed outward along the longer wall.

5.3. *Reynolds-stress principal planes*

Consider any cubical fluid element in a general turbulent-flow field, aligned with the x-direction, but not necessarily fixed with respect to the y- and z-axes. The Reynolds shear stresses acting along faces parallel to the x-direction in directions normal to the x-direction are defined as $\rho\overline{u_2 u_3}$ stresses, where ρ is the fluid density and $\overline{u_2 u_3}$ is a one-point correlation of mutually perpendicular velocity fluctuations, u_2 and u_3, in a plane normal to the x-direction. At any point in the flow field, a $\rho\overline{u_2 u_3}$ type of stress can act on a fluid element for an infinite number of element orientations. There are only certain orientations of the element, however, for which $\rho\overline{u_2 u_3} = 0$. Under these circumstances, when element faces parallel to the x-direction are projected onto a yz-plane, the projections represent traces of principal planes. In this investigation measurements were taken in order to determine whether traces of these planes are tangent and normal to isotachs for fully-developed turbulent flow in a rectangular channel. This work represents an extension of earlier work by Gessner & Jones (1961), who concluded that such traces are tangent and normal to isotachs for rectangular channel flow with zero pressure gradient. In further discussion we shall examine the quantity $\overline{u_2 u_3}$ since its behaviour is indicative of the behaviour of $\rho\overline{u_2 u_3}$ for incompressible flow.

In accordance with a method described by Gessner (1964*b*), $\overline{u_2 u_3}$ measurements were made in the square channel at selected points along an isotach on planes normal and tangent to the isotach and on planes oriented $\pm 20°$ with respect to these planes. The results are shown in figure 9; for clarity only normal planes and planes oriented $\pm 20°$ from the normal planes are shown in the figure. The sign ($+$ or $-$) of $\overline{u_2 u_3}/U_0^2$ measured on each plane was determined by applying a co-ordinate-axes transformation to the Reynolds stresses acting on a fluid element located on the wall bisector parallel to the y-axis, and oriented with respect to the xyz co-ordinate system. In order to determine the traces shown in figure 9, the value $\overline{u_2 u_3}/U_0^2 = 0$ was interpolated from measured values for the different plane orientations at each point. The results indicate that traces of principal planes in a yz-plane are definitely not tangent and normal to isotachs. Further measurements taken in the square channel at $Re = 300{,}000$ confirmed this behaviour. The above-mentioned results discount the findings of Gessner & Jones (1961) because they are based on an improved measuring technique. The results also show that the assumption of no Reynolds shear stresses on planes

normal to isotachs, used by Deissler & Taylor (1959) in their theoretical investigation of turbulent channel flow, is invalid.

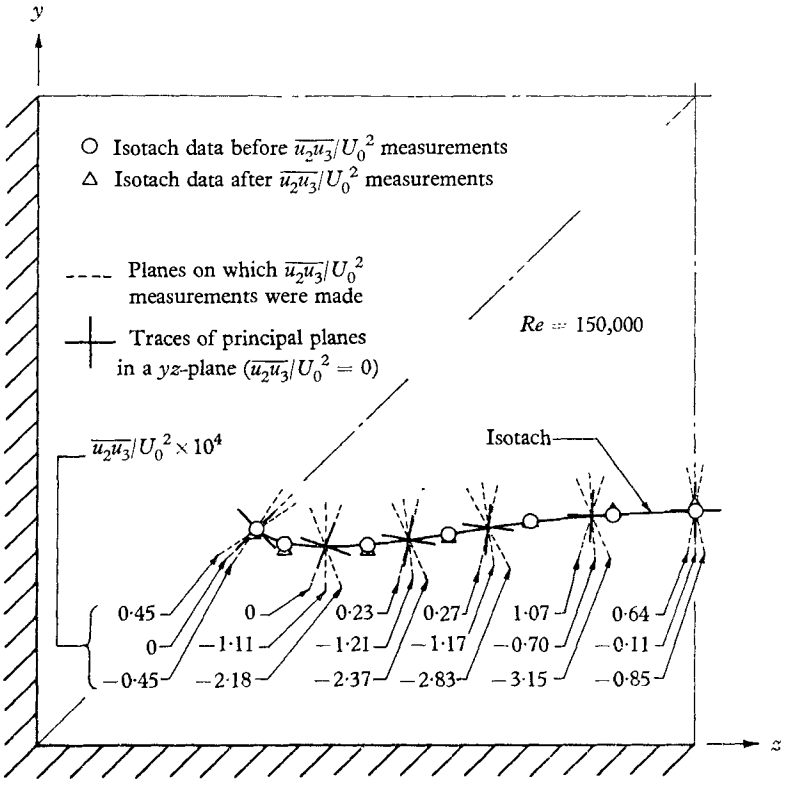

FIGURE 9. $\overline{u_2u_3}/U_0^2$ values at points along an isotach.

5.4. *Momentum balance along a secondary-flow streamline*

It is sometimes more convenient to describe complex flows in terms of natural co-ordinates rather than conventional x, y, z co-ordinates. For the particular case of turbulent flow in non-circular channels it is expedient to express the Reynolds equations in terms of a co-ordinate system based on secondary-flow streamlines. Let an orthogonal curvilinear co-ordinate system be defined in terms of x, s and n, where x is in the axial flow direction, s is along secondary-flow streamlines, and n is along normals to these streamlines. If the Reynolds equations are written in terms of this system, then the equation in the s-direction describes the motion of fluid along secondary-flow streamlines. At this point we shall limit ourselves to a derivation of the Reynolds equation along one particular secondary-flow streamline whose configuration is known from integration of measured secondary-flow profiles. This streamline is designated as streamline A for future reference. Experimental evaluation of the various terms in the Reynolds equation along streamline A should provide sufficient information to permit determination of the driving mechanisms causing secondary flow in general.

An assumption will now be made which simplifies the Reynolds equation along

streamline A considerably, namely that the curvature of normals to streamlines adjacent to streamline A is zero. This assumption is justified if streamlines adjacent to streamline A are approximately equidistant from each other. The results of Hoagland (1960) substantiate this assumption because they indicate that near secondary-flow cell boundaries streamlines are approximately equidistant, except in the vicinity of a corner. Although the above assumption is equivalent to an assumption of no convergence or divergence of streamlines adjacent to streamline A, we will still admit, however, that a fluid particle on streamline A can be either accelerated or decelerated along the streamline.

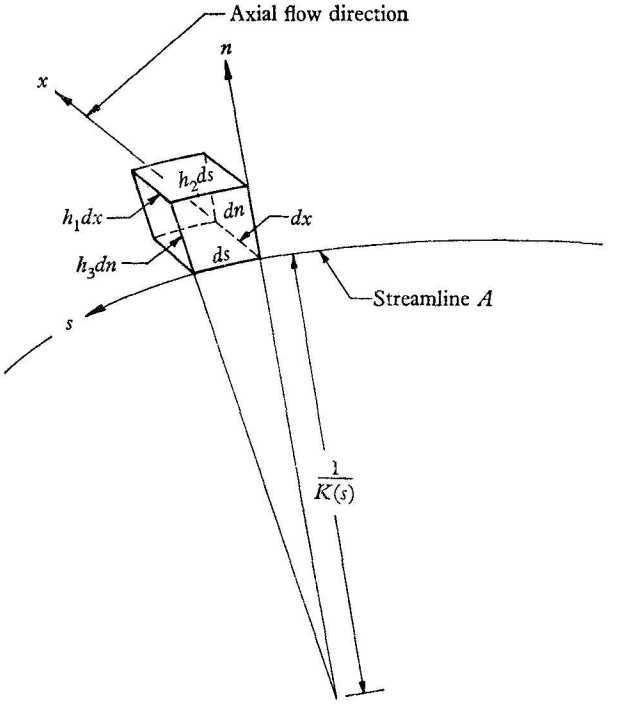

FIGURE 10. Orthogonal curvilinear co-ordinate system.

Consider now steady, incompressible, fully-developed turbulent flow in a non-circular channel. Let the xsn co-ordinate system defined above be located with respect to streamline A as shown in figure 10. In reference to the fluid element shown in the figure, the quantities h_1, h_2, and h_3 are normally functions of x, s and n in a general orthogonal curvilinear co-ordinate system. Because the flow is considered to be fully developed, however, h_1 is unity. Furthermore, h_3 is also unity because streamlines adjacent to streamline A are assumed to be equidistant from each other. The quantity h_2 is a function of $K(s)$ and n, where K is a function of s alone because it is referred to streamline A. From similarity of curvilinear triangles in figure 10 we have

$$\frac{h_2 ds}{(1/K)+n} = \frac{ds}{1/K}, \tag{1}$$

or

$$h_2 = 1 + Kn. \tag{2}$$

In accordance with Townsend (1956, pp. 30–31), for example, and the assumptions mentioned thus far, the continuity equation for the mean flow and the Reynolds equation along streamline A can be written respectively as:

$$\frac{\partial U_s}{\partial s}+\frac{\partial(h_2 U_n)}{\partial n}=0, \tag{3}$$

$$\frac{U_s}{h_2^2}\frac{\partial(h_2 U_s)}{\partial s}+\frac{U_n}{h_2}\frac{\partial(h_2 U_s)}{\partial n}-\frac{U_s^2+\overline{u_s^2}}{h_2^2}\frac{\partial h_2}{\partial s}+\frac{1}{h_2^2}\left[\frac{\partial(h_2\overline{u_s^2})}{\partial s}+\frac{\partial(h_2^2\overline{u_s u_n})}{\partial n}\right]$$
$$+\frac{1}{\rho h_2}\frac{\partial P}{\partial s}+\nu\left[\frac{\partial}{\partial n}\left(\frac{1}{h_2}\frac{\partial U_n}{\partial s}\right)-\frac{\partial}{\partial n}\left\{\frac{1}{h_2}\frac{\partial(h_2 U_s)}{\partial n}\right\}\right]=0, \tag{4}$$

where U_s and U_n are mean velocity components in the s- and n-directions, respectively, and P is the mean static pressure. The quantity $\overline{u_s u_n}$ is a one-point correlation between u_s and u_n, the instantaneous velocity fluctuations in the s- and n-directions, respectively, and $\overline{u_s^2}$ is the time-averaged value of the square of u_s.

If (3) is introduced into (4) and gradients of h_2 are evaluated, (4) becomes

$$\frac{U_s}{h_2}\frac{\partial U_s}{\partial s}+U_n\frac{\partial U_s}{\partial n}+\frac{KU_sU_n}{h_2}+\frac{1}{\rho h_2}\frac{\partial P}{\partial s}$$
$$-\nu\left(\frac{1}{h_2^2}\frac{\partial^2 U_s}{\partial s^2}+\frac{\partial^2 U_s}{\partial n^2}+\frac{K}{h_2}\frac{\partial U_s}{\partial n}-\frac{K^2 U_s}{h_2^2}+\frac{2K}{h_2^2}\frac{\partial U_n}{\partial s}+\frac{n}{h_2^2}\frac{\partial K}{\partial s}\frac{\partial U_n}{\partial n}+\frac{U_n}{h_2^2}\frac{\partial K}{\partial s}\right)$$
$$+\frac{1}{h_2}\frac{\partial\overline{u_s^2}}{\partial s}+\frac{\partial\overline{u_s u_n}}{\partial n}+\frac{2K\overline{u_s u_n}}{h_2}=0. \tag{5}$$

Equation (5) can be simplified further by noting that, along streamline A, the variables n and U_n are zero everywhere and h_2 is equal to unity. On the basis of these considerations (5) can be written as

$$U_s\frac{\partial U_s}{\partial s}+\frac{1}{\rho}\frac{\partial P}{\partial s}-\nu\left(\frac{\partial^2 U_s}{\partial s^2}+\frac{\partial^2 U_s}{\partial n^2}+K\frac{\partial U_s}{\partial n}-K^2U_s\right)+\frac{\partial\overline{u_s^2}}{\partial s}+\frac{\partial\overline{u_s u_n}}{\partial n}+2K\overline{u_s u_n}=0. \tag{6}$$

Equation (6) will now be written in dimensionless form. Let

$$U_s^*=U_s/U_b, \qquad s^*=s/D_h,$$
$$\overline{u_s^2}^*=\overline{u_s^2}/U_b^2, \qquad n^*=n/D_h,$$
$$\overline{u_s u_n}^*=\overline{u_s u_n}/U_b^2, \qquad K^*=KD_h,$$
$$P^*=P/\rho U_b^2, \qquad Re=U_b D_h/\nu.$$

Equation (6) therefore becomes

Convection Pressure Viscous

$$U_s^*\frac{\partial U_s^*}{\partial s^*}+\frac{\partial P^*}{\partial s^*}-\frac{1}{Re}\left(\frac{\partial^2 U_s^*}{\partial s^{*2}}+\frac{\partial^2 U_s^*}{\partial n^{*2}}+K^*\frac{\partial U_s^*}{\partial n^*}-K^{*2}U_s^*\right)$$

Turbulence

$$+\left(\frac{\partial\overline{u_s^2}^*}{\partial s^*}+\frac{\partial\overline{u_s u_n}^*}{\partial n^*}+2K^*\overline{u_s u_n}^*\right)=0. \tag{7}$$

The terms commonly referred to as convection, pressure, viscous, and turbulence terms are indicated in (7). It must be re-emphasized that (7) applies only along streamline A and not elsewhere in the flow field because of the limiting nature of the assumptions used in the derivation.

In order to examine fluid motion along secondary-flow streamlines, a streamline map was constructed from the secondary-flow profiles shown in figure 4 in accordance with the method discussed below. Subsequently, a streamline was chosen for further study (streamline A), and mean-flow and turbulence measurements were made with respect to this streamline in order to evaluate the terms of (7).

For the particular case of steady, fully-developed turbulent flow in a square channel let a dimensionless stream function Ψ be defined in terms of the channel half-width, a, the centreline velocity, U_0, and the secondary-flow components in the y- and z-directions, V and W, respectively, as follows:

$$\frac{V}{U_0} = \frac{\partial \Psi}{\partial (z/a)}, \quad \frac{W}{U_0} = \frac{-\partial \Psi}{\partial (y/a)}. \tag{8}$$

Since $\Psi(y, z)$ has continuous first partial derivatives everywhere in the flow field,

$$d\Psi = \frac{\partial \Psi}{\partial (y/a)} d(y/a) + \frac{\partial \Psi}{\partial (z/a)} d(z/a). \tag{9}$$

Comparing (8) and (9), one obtains

$$d\Psi = \frac{-W}{U_0} d(y/a) + \frac{V}{U_0} d(z/a). \tag{10}$$

As mentioned earlier, secondary-flow streamlines in the square channel are based on integration of the W/U_0 profiles shown in figure 4. Since these profiles lie along lines $z/a = \text{const.}$, (10) can be reduced to

$$d\Psi = \frac{-W}{U_0} d(y/a), \tag{11}$$

from which it follows that

$$\Psi = -\int_0^{y'/a} \frac{W}{U_0} d(y/a), \tag{12}$$

where y'/a is a dimensionless distance from the wall $y = 0$.

By numerical integration of (12) the secondary-flow streamlines shown in figure 11 were evaluated. The profiles in figure 4 were integrated from the diagonal to the wall, primarily because of the uncertainty of profile configurations very near the wall. The streamline selected for further study was the streamline $\Psi = 8 \times 10^{-4}$ shown in figure 11. To check the configuration of this streamline, resultant secondary-flow velocities were calculated along the streamline from measured components at selected points on the streamline. The results indicated that the resultant velocities were everywhere approximately tangent to the streamline.

After the configuration of the streamline had been verified, the various terms of (7) were evaluated. The convection and viscous terms were determined first by interpolating W/U_0 values at selected points along and normal to the streamline from the profiles shown in figure 4. Each interpolated component was then projected onto a line parallel to or coincident with a tangent to the streamline in order to determine the resultant secondary-flow velocity, U_s. At points along

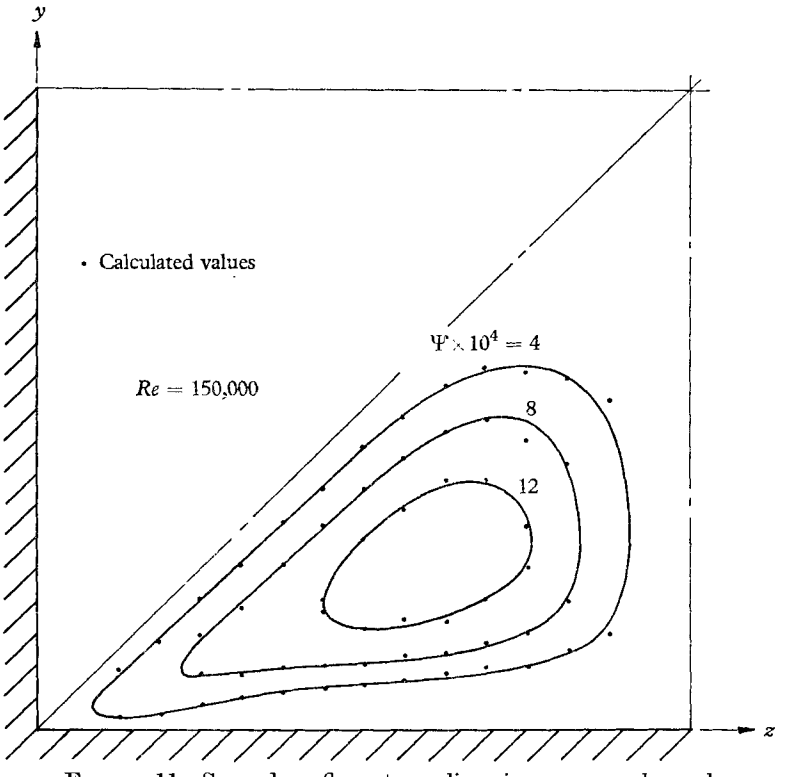

FIGURE 11. Secondary-flow streamlines in a square channel.

the streamline the curvature, K, was also measured. By plotting gradients of U_s along and normal to the streamline, and non-dimensionalizing the results, such quantities as $U_s^* \partial U_s^*/\partial s^*$, $\partial^2 U_s^*/\partial n^{*2}$, and $K^* \partial U_s^*/\partial n^*$ were determined. Subsequently, by summing quantities in accordance with (7), the convection and viscous terms were evaluated.

The behaviour of the convection term can be seen in figure 12. The reference value $s^* = 0$ was arbitrarily chosen as the point where a fluid particle begins acceleration toward the corner. The calculated values from which the plot was made are shown by dots. It is seen that a fluid particle is accelerated toward the corner bisector from the origin, moves with approximately constant velocity near the corner bisector, and is decelerated very rapidly in the corner region. The particle is then accelerated away from the corner, at first rapidly, then less rapidly, until it is decelerated as it moves along the wall toward the wall bisector. The deceleration continues until the particle moves with approximately constant

velocity as it approaches the origin again. The behaviour of a fluid particle along the streamline is in accordance with predictable behaviour based on the convergence and divergence of streamlines shown in figure 11.

Figure 13 shows the influence of the viscous stresses on the motion of a fluid particle along the streamline. The fluid motion is affected primarily by the quantity $-(1/Re)\,\partial^2 U_s^*/\partial s^{*2}$, to a much lesser degree by $(K^{*2}/Re)\,U_s^*$, and

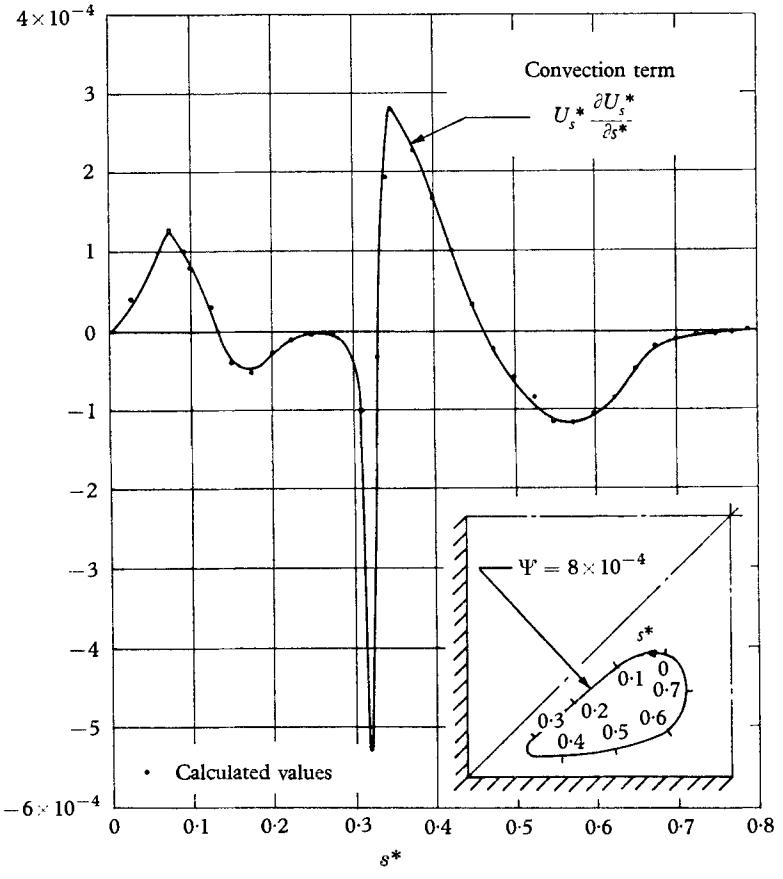

FIGURE 12. Convection term in the Reynolds equation along the streamline $\Psi = 8 \times 10^{-4}$.

negligibly by the other quantities. A comparison of figures 12 and 13 shows that the viscous stresses alone cannot sustain secondary flow, because the influence of these stresses is confined to the corner region. In accordance with (7), therefore, it follows that secondary flow must be the result of forces exerted by static pressure gradients and the Reynolds stresses in planes normal to the axial flow direction. In order to determine the relative magnitudes of these forces, the pressure and turbulence terms in (7) were evaluated in accordance with the following considerations.

The turbulence term in (7) was determined by making measurements along and normal to the streamline. Figures 14 and 15 show $\overline{u_s^2}^*$ and $\overline{u_s u_n}^*$ distributions,

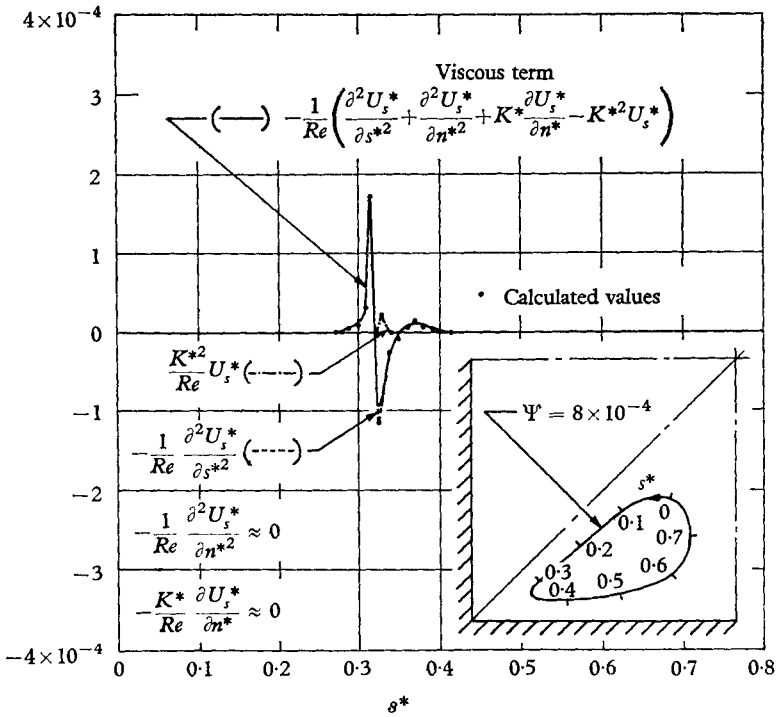

FIGURE 13. Viscous term in the Reynolds equation along the streamline $\Psi = 8\times10^{-4}$.

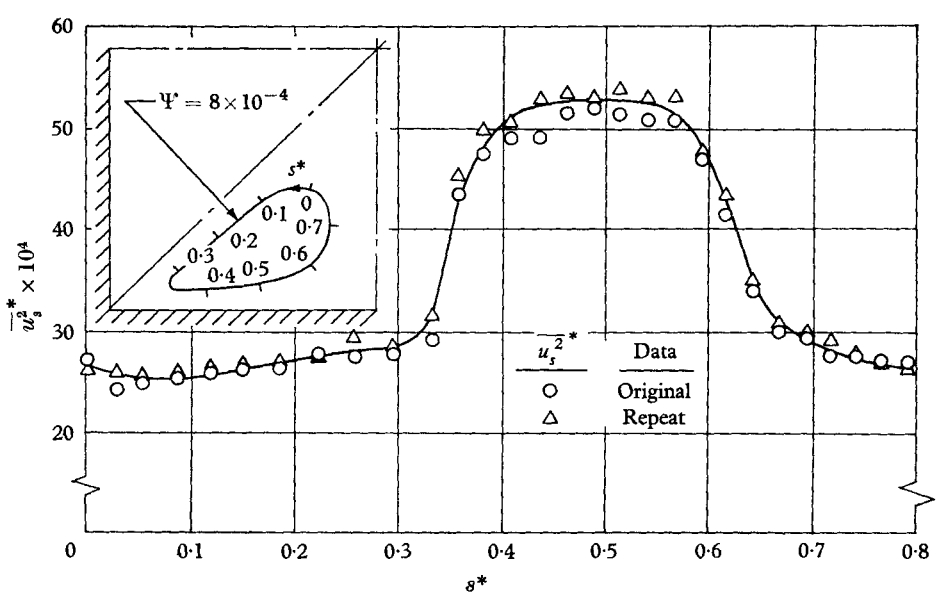

FIGURE 14. $\overline{u_s^{2*}}$ variation with s^* along the streamline $\Psi = 8\times10^{-4}$.

respectively, which were measured by a 'follow the streamline' technique; that is, by making continuous measurements at successive points along the streamline. Both 'original' and 'repeat' data were taken in order to plot distributions as accurately as possible. For $\overline{u_s^2}^*$ measurements the plane of the X-array was aligned tangentially to the streamline. Measurements of $\overline{u_s u_n}^*$ were made by orienting the plane of the X-array $\pm 45°$ with respect to normals to the streamline in accordance with the method discussed by Gessner (1964*b*). The sign of $\overline{u_s u_n}^*$ (+ or −) was determined by applying a co-ordinate-axes transformation to the

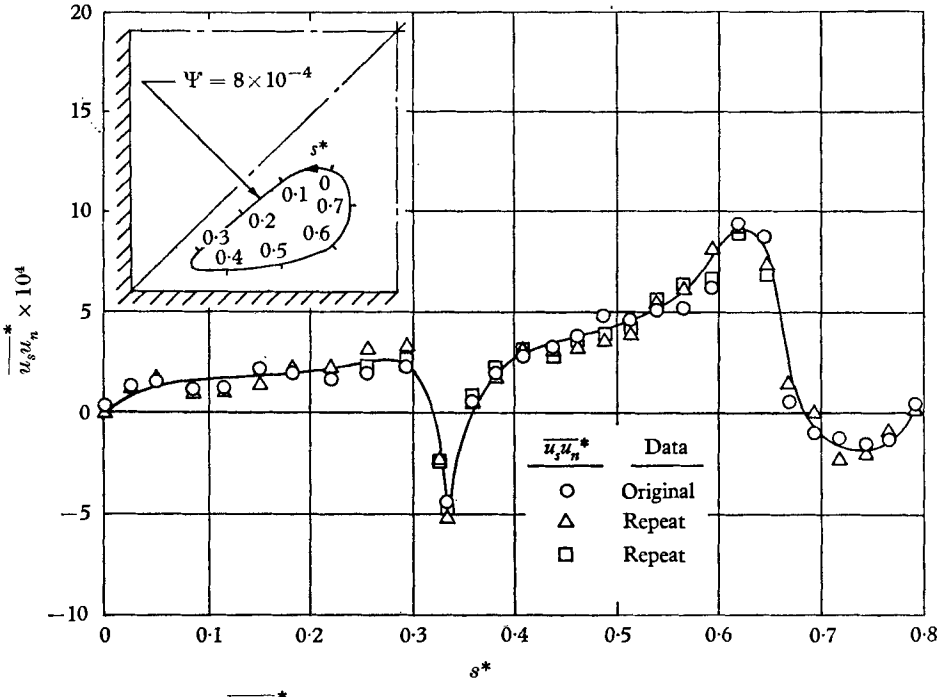

FIGURE 15. $\overline{u_s u_n}^*$ variation with s^* along the streamline $\Psi = 8 \times 10^{-4}$.

Reynolds stresses acting on fluid elements located at selected points along the streamline and oriented with respect to the xyz co-ordinate system.

The variation of $\overline{u_s u_n}^*$ along normals to the streamline is shown in figures 16 and 17. In order to determine normal gradients of $\overline{u_s u_n}^*$, measurements were taken initially at selected points along the streamline and at distances $\pm 0{\cdot}20$ in. along normals to the streamline at these points. The measurements were taken by using a 'follow the normal' technique. At $s^* = 0{\cdot}221$ and $0{\cdot}257$ it was noted that normal gradients could not be determined on the basis of measurements at intervals of $\pm 0{\cdot}20$ in.; this is evident from the dashed-line distributions shown in figure 16. To circumvent this difficulty, subsequent measurements were made at shorter distance increments along normals, specifically at increments of $\pm 0{\cdot}05$ in. from the streamline. Measured values of $\overline{u_s u_n}^*$ based on the new distance increments were sufficiently well behaved to permit the evaluation of the $\overline{u_s u_n}^*$ normal gradients shown in figures 16 and 17. It should be mentioned

that the data shown in the figures were most difficult to obtain and required considerable time and effort.

With reference to the turbulence term in (7), the quantity $\partial \overline{u_s^2}^*/\partial s^*$ was evaluated by calculating gradients at selected points along the distribution shown in figure 14. The quantity $2K^*\overline{u_s u_n}^*$ was determined at points along the distribution shown in figure 15 after streamline curvature had been measured at

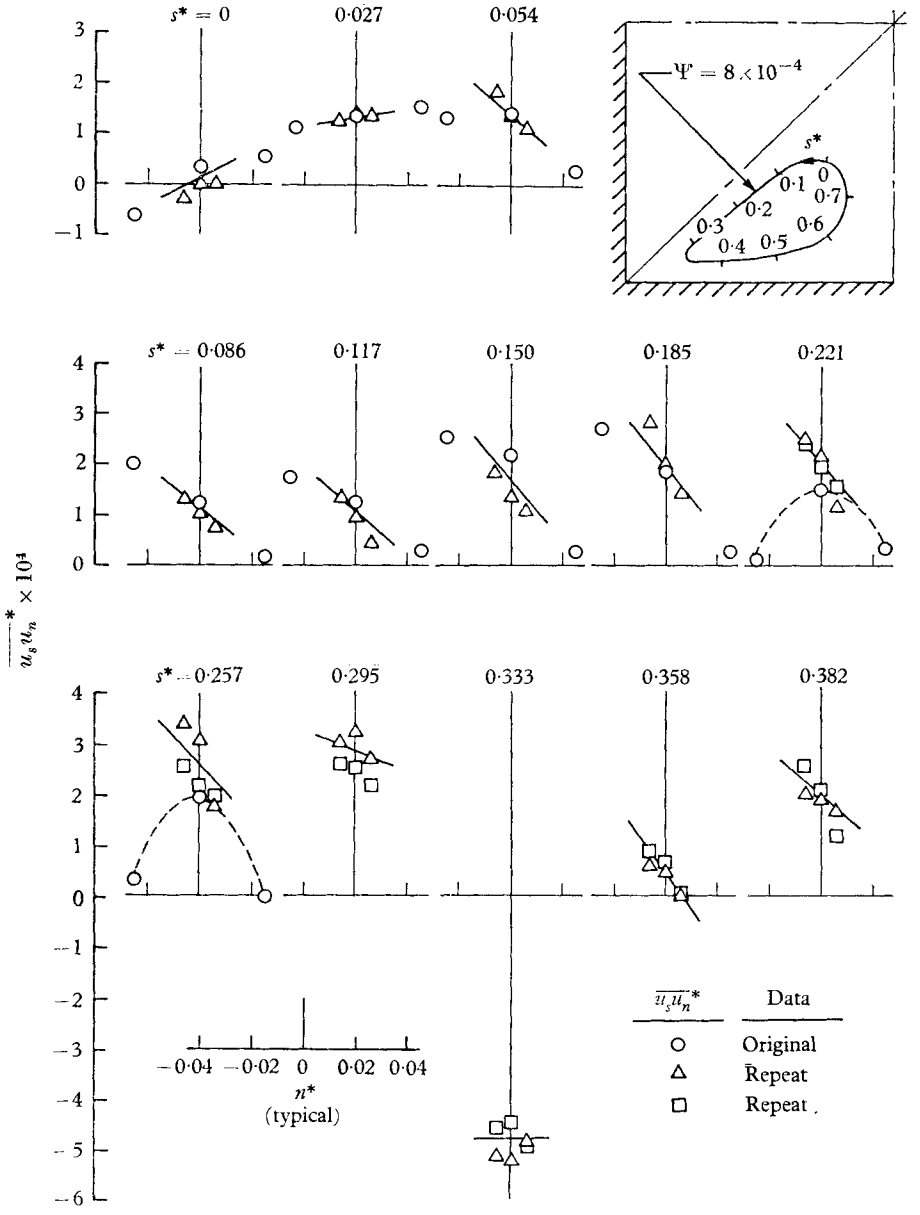

FIGURE 16. $\overline{u_s u_n}^*$ variation along normals to the streamline $\Psi = 8 \times 10^{-4}$ $(0 \leqslant s^* \leqslant 0{\cdot}382)$.

each of these points. Finally, the normal gradient $\partial \overline{u_s u_n}^* / \partial n^*$ was evaluated at each of the s^* points indicated in figures 16 and 17. The individual turbulence quantities and sum of quantities in accordance with (7) are shown in figure 18. The behaviour of the individual quantities is complicated; however, it is evident that the largest turbulent stress variations along the streamline exist in the immediate vicinity of the corner. Further discussion of these quantities follows shortly when the overall momentum balance is discussed.

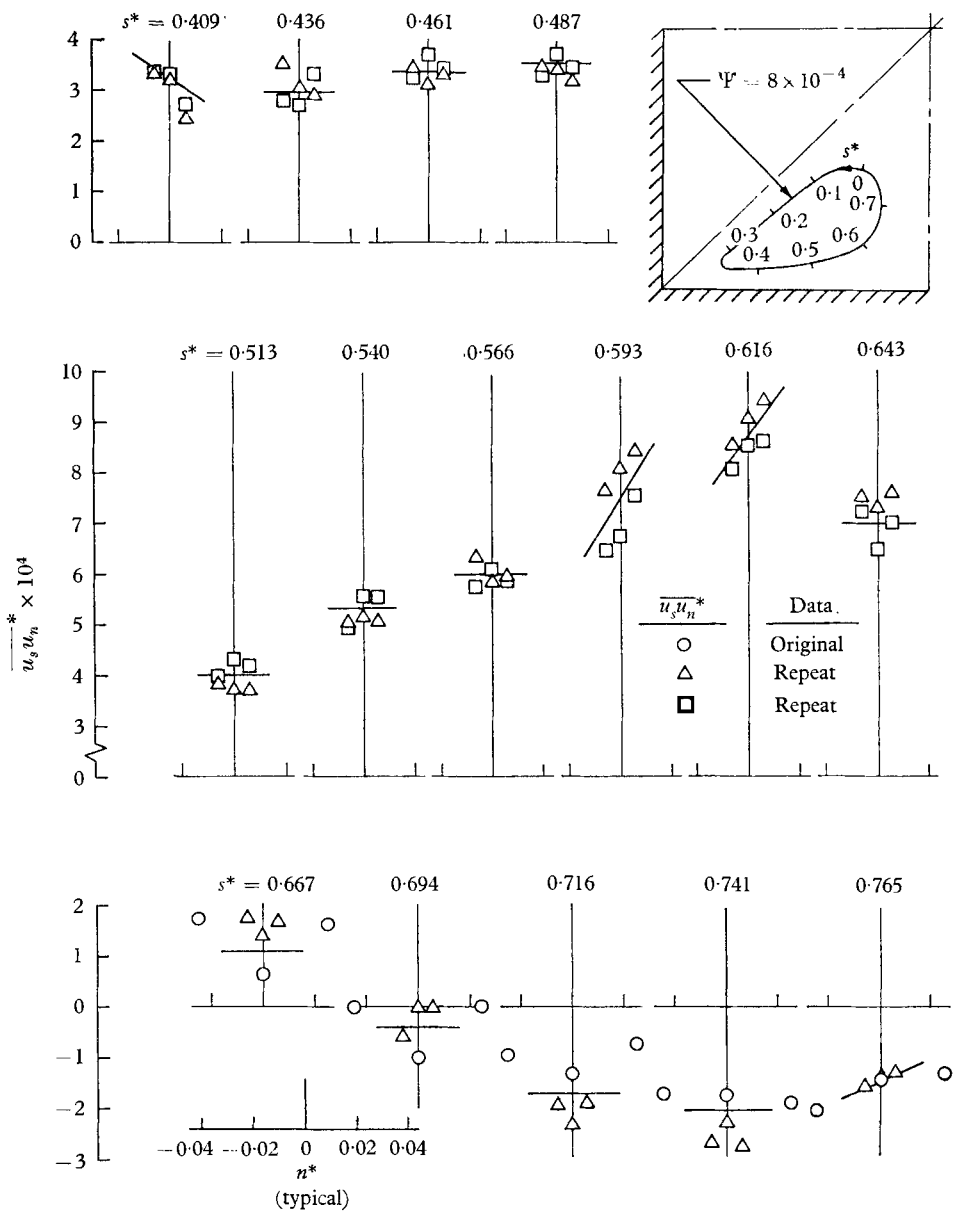

FIGURE 17. $\overline{u_s u_n}^*$ variation along normals to the streamline $\Psi = 8 \times 10^{-4}$ ($0{\cdot}409 \leqslant s^* \leqslant 0{\cdot}765$).

In order to evaluate the static-pressure gradient along the streamline, measurements were taken with a Pitot static tube at selected points on the streamline. These measurements indicated a static-pressure variation of less than 0·001 in. of water. Higher accuracy measurements were not attempted because of the influence of corner effects and turbulence intensity on static-pressure readings. Therefore, since the static-pressure gradient was not measured explicitly, the pressure term is used as a closing entry in (7).

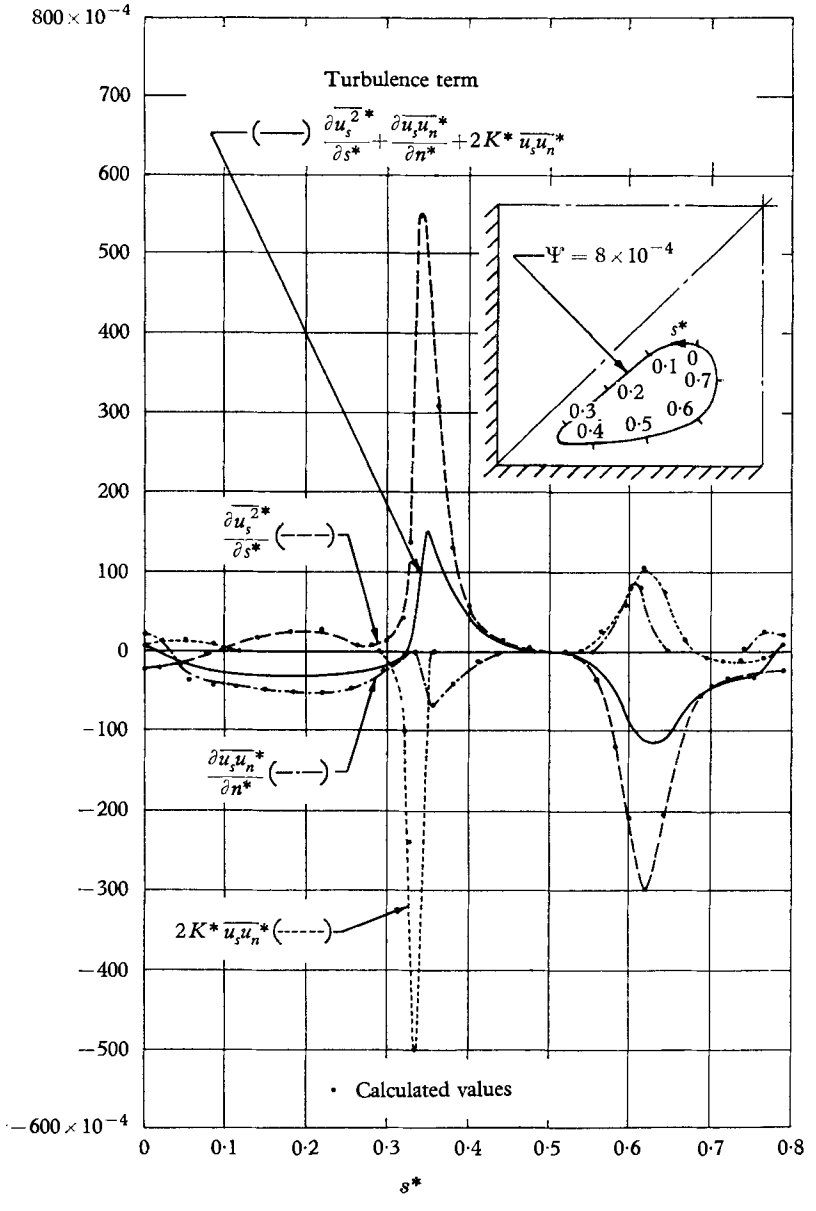

FIGURE 18. Turbulence term in the Reynolds equation along the streamline $\Psi = 8 \times 10^{-4}$.

The momentum balance along the streamline is shown in figure 19, and is based on the distributions shown in figures 12, 13 and 18. In figure 19 the turbulence term is shown in two parts representing separately the normal- and shear-stress quantities which appear to balance approximately along part of the stream-

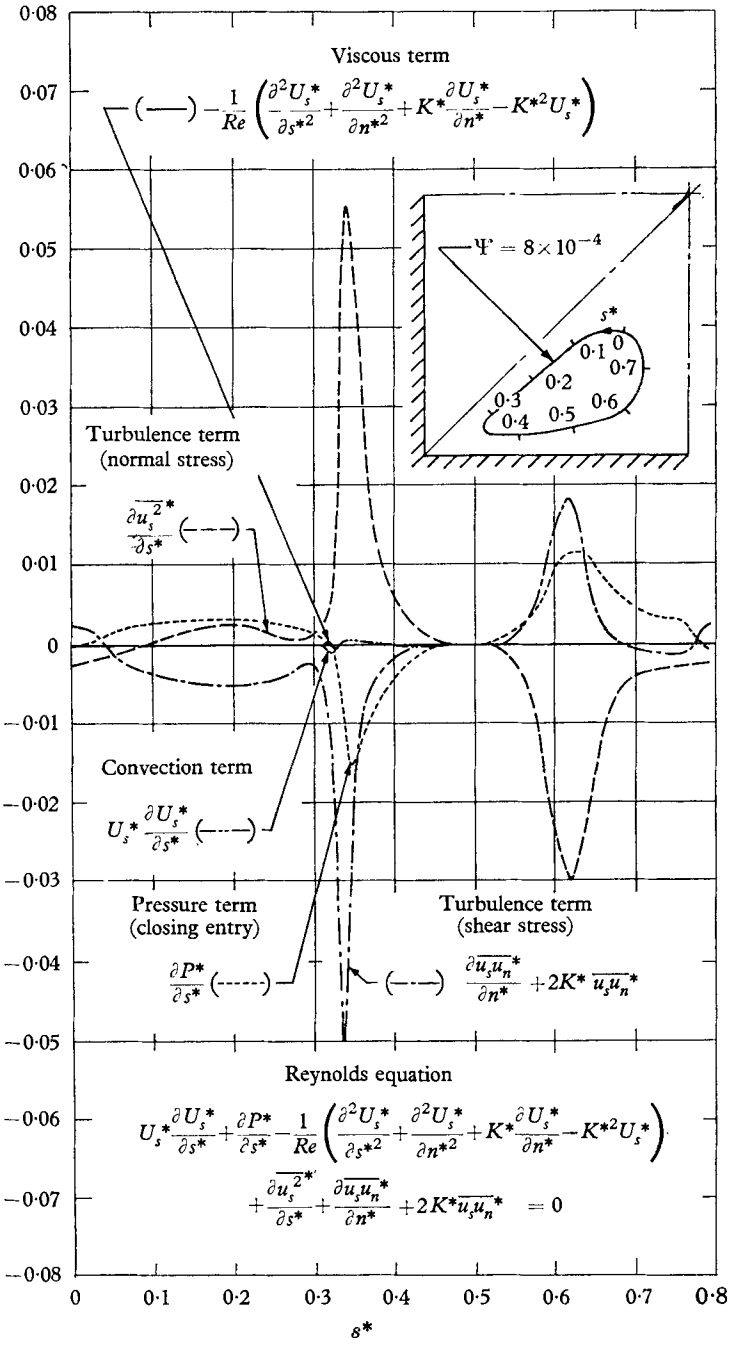

FIGURE 19. Momentum balance along the streamline $\Psi = 8\times10^{-4}$.

line. The pressure term is a closing entry, and therefore its apparent variation is somewhat questionable, especially since it is based essentially on difficult-to-measure turbulence quantities. However, it should be noted that the behaviour of the pressure term in the interval $0{\cdot}63 \leqslant s^* \leqslant 0{\cdot}79$ ($\partial P^*/\partial s^*$ positive and decreasing with increasing s^*) is in accordance qualitatively with predictable behaviour based on an exact solution to the Reynolds equations for turbulent flow in a two-dimensional channel and Laufer's measurements (1951) in the same geometry. Furthermore, the maximum value of the closing entry ($\partial P^*/\partial s^* \approx 10^{-2}$) corresponds to a static pressure gradient of less than 0·0007 in. of water per inch of length along the streamline, thus giving further confidence in the turbulence measurements and, consequently, in the pressure term as a closing entry.

It is not possible to state explicitly the exact manner in which fluid-particle convection along secondary-flow streamlines is influenced by transverse static-pressure gradients and the Reynolds stresses, since the convection term is approximately two orders of magnitude less than either the pressure or turbulence term. One can conclude only that secondary flow is the result of complex interactions between the Reynolds stresses and the static pressure.

Although the momentum balance shown in figure 19 is along one particular streamline, the balance is indicative of the viscous, pressure and turbulence stresses influencing fluid motion along other secondary-flow streamlines. Of course, fluid motion along streamlines very near the wall is more likely to be influenced by the viscous stresses; however, in this region Reynolds-stress gradients and static-pressure gradients are also large, and consequently the basic character of the balance is likely to be unchanged.

6. Conclusions

On the basis of the above results, the following conclusions are drawn for fully-developed turbulent flow in straight rectangular channels. In particular, the conclusions apply to flow in a square channel between Reynolds numbers of 75,000 and 300,000 and to flow in a 2×1 rectangular channel between Reynolds numbers of 50,000 and 300,000.

1. Secondary-flow velocities, when non-dimensionalized with either the bulk velocity or the channel-centreline mean-flow velocity, decrease for an increase in Reynolds number.

2. The greatest skewness of local wall shear-stress vectors occurs in the immediate vicinity of corners. For rectangular channels the skewness on the longer wall is greater than the skewness on the shorter wall at points equidistant from the corner.

3. In planes normal to the axial flow direction, traces of Reynolds-stress principal planes are not tangent and normal to isotachs. This behaviour is in contrast to that for turbulent flow in two-dimensional channels and circular pipes, where such traces are always tangent and normal to isotachs in accordance with symmetry considerations.

4. In planes normal to the axial-flow direction, opposing forces are exerted by (i) the Reynolds stresses and (ii) static-pressure gradients. Small differences in magnitude of these forces cause secondary flow.

REFERENCES

BRUNDRETT, E. 1964 The production and diffusion of vorticity in duct flow. *J. Fluid Mech.* **19**, 375.

DEISSLER, R. G. & TAYLOR, M. F. 1959 Analysis of turbulent flow and heat transfer in noncircular passages. *NASA TR*, no. R-31.

GESSNER, F. B. 1964*a* Turbulence and mean-flow characteristics of fully-developed flow in rectangular channels. Doctoral thesis, Purdue University.

GESSNER, F. B. 1964*b* A method of measuring Reynolds stresses with a constant-current, hot-wire anemometer. *ASME Paper*, 64-WA/FE-34.

GESSNER, F. B. & JONES, J. B. 1961 A preliminary study of turbulence characteristics of flow along a corner. *J. Basic Engng, Trans. ASME*, **83**, 657.

GILBERT, G. B. 1960 Secondary flow in straight rectangular ducts. Master's Thesis, Massachusetts Institute of Technology.

HOAGLAND, L. C. 1960 Fully-developed turbulent flow in straight rectangular ducts—secondary flow, its cause and effect on the primary flow. Doctoral Thesis, Massachusetts Institute of Technology.

LAUFER, JOHN 1951 Investigation of turbulent flow in a two-dimensional channel. *NACA TR*, no. 1053.

LEUTHEUSSER, H. J. 1963 Turbulent flow in rectangular ducts. *J. Hyd. Div., Proc. ASCE*, **89**, 1.

MASLEN, S. H. 1958 Transverse velocities in fully-developed flows. *Quart. Appl. Math.* **16**, 173.

MOISSIS, R. 1957 Secondary flow in rectangular ducts. Master's Thesis, Massachusetts Institute of Technology.

NIKURADSE, J. 1926 Untersuchungen über die Geschwindigkeitsverteilung in turbulenten Strömungen. *V.D.I. Forschungsheft*, **70**, 1229.

OMAN, R. A. 1959 The three-dimensional laminar boundary layer along a corner. Doctoral Thesis, Massachusetts Institute of Technology.

ROSE, W. G. 1962 *Symposium on Measurement in Unsteady Flow*, pp. 85–9. *ASME* publication.

TOWNSEND, A. A. 1956 *The Structure of Turbulent Shear Flow*. Cambridge University Press.